Simulations and density functional calculations of surface forces in the presence of semiflexible polymers

Martin Turesson,* Jan Forsman, and Torbjörn Åkesson
Theoretical Chemistry, Chemical Centre, P.O. Box 124, S-221 00 Lund, Sweden
(Received 3 May 2007; published 7 August 2007)

We simulate interactions between adsorbing and nonadsorbing surfaces immersed in solutions containing monodisperse semiflexible chains. Apart from the nature of the surfaces, we investigate responses to changes of the intrinsic chain stiffness, the degree of polymerization, and the bulk concentration. Our simulations display a sufficient accuracy and precision to reveal free-energy barriers that are small on a typical scale of surface force simulations, but still of the same order as the expected van der Waals interactions. Two different approaches have been tested: grand canonical simulations, improved by configurational-biased techniques, and a perturbation method utilizing the isotension ensemble. We find the former to be preferable when the surfaces are nonadsorbing, whereas the isotension approach is superior for calculations of interactions between adsorbing surfaces, especially if the polymers are stiff. We also compare our simulation results with predictions from several versions of polymer density functional theory. We find that a crucial aspect of these theories, in quantitative terms, is that they recognize that end monomers exclude more volume to the surrounding than inner ones do. Those theories provide satisfactorily accurate predictions, particularly when the surfaces are nonadsorbing.

DOI: 10.1103/PhysRevE.76.021801 PACS number(s): 61.25.Hq, 68.03.Cd, 05.70.Np, 82.70.Dd

I. INTRODUCTION

Experimentally, a lot of attention has been paid to understanding and characterizing the forces between surfaces immersed in polymer solutions [1–6]. The ability of polymers to stabilize or destabilize colloidal particles in solution makes them candidates for a wide range of applications. The surface force apparatus and atomic force microscopy are frequently used to study surface forces between two closely separated surfaces. Except for technical difficulties, a major concern is the often slow establishment of diffusive equilibrium—i.e., slow transfer of polymers between the intersurface region and the bulk reservoir [7].

Comparisons with simulated surface forces are rare in the literature. Simulations also suffer from difficulties related to bulk exchange, as dictated by the requirement of a constant chemical potential as the surface separation is changed. The most obvious approach in such studies is to simulate in the grand canonical ensemble (GCE). However, the acceptance probability of insertion or deletion decreases rapidly with polymer length. The polymer excess chemical potential can be evaluated by thermodynamic integration [8], whereby the acceptance problem is partly circumvented, but many simulations are then required. Another related approach is to gradually build up the chain monomer by monomer and calculate individual incremental contributions to the total chemical potential [9,10].

By using a biased sampling technique introduced by Rosenbluth and Rosenbluth [11], Harris and Rice [12], as well as Siepmann and Frenkel [13], was able to calculate the excess chemical potential for a polymer with discrete conformations in a lattice model, using a single simulation. Subsequently, Frenkel *et al.* [14,15] and de Pablo *et al.* [16,17] made analogous simulations for a continuously deformable chain molecule. The idea of this so-called configurational-biased Monte Carlo method is to enhance the insertion probability for a chain molecule by stepwise insertion. Starting with monomer i, Boltzmann weights for a small number of spatial coordinates for monomer $i+1$ are calculated. One of these positions is then chosen, with a probability given by its Boltzmann weight, to be the actual coordinate of monomer $i+1$. The process is repeated until the whole chain has been built up.

In this work we have simulated surface forces in a slit geometry, for systems containing semi-flexible hard sphere polymers, of various lengths (10–30 monomers/chain). We have focused on how the surface interactions respond to changes of the intrinsic stiffness of the chains and (for adsorbing surfaces) the bulk monomer concentration. We have also evaluated two different simulation techniques.

The equilibrium criterion implies that the polymer chemical potential is conserved, as the surface separation is changed. This is either accomplished by the configurational-biased Monte Carlo method described above—i.e., by GCE simulations—or by adopting a free-energy difference method (FEDM), which utilizes the isotension ensemble (IE) [18]. This FEDM technique was introduced by Svensson and Woodward [19,20]. Forsman and Woodward [21] subsequently optimized the performance of this approach by implementing an IE version of Bennett's rate method [22]. In IE simulations, the area of the simulation box—i.e., the density of polymers—is regulated by an external pressure applied in the direction parallel to the surfaces. Changing the surface-surface separation requires a mutual change in the parallel pressure in order to keep the chemical potential constant [19–21,23]. The expanded IE, implemented by Broukhno *et al.* [24], is a similar technique, although it is based on real, rather than virtual, perturbations. A drawback is that it lacks the considerable performance enhancement

*martin.turesson@teokem.lu.se

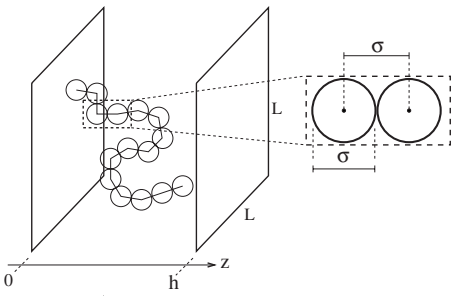

FIG. 1. The polymers are modeled as hard spheres of diameter σ connected by rigid bonds of length σ (see dashed box). The quadratic surfaces with side length L are located in $z=0$ and $z=h$.

offered by the variance minimization procedure [21,22]. Still, it has been successfully used to study surface forces [24–26].

In the presence of nonadsorbing (monomer-repelling) surfaces, we found the GCE approach to be preferable, at least for the rather short chains we have investigated. When the surfaces are strongly adsorbing, however, the GCE method fails to provide a precision high enough to allow detection and quantification of free-energy barriers. In those cases, the IE technique was superior. With this approach, we are still able to detect free-energy barriers that are *remarkably small* on an absolute scale, but still relevant, in the sense that they are comparable in magnitude to a typical van der Waals attraction. They would furthermore be detected in a typical surface force apparatus (SFA) or atomic force microscopy (AFM) experiment.

In addition to these simulation studies, we have also compared a number of density functional versions, based on Woodward's formulation [27]. Some of these have been established previously, while others are tested here. The different versions are evaluated by comparing surface force predictions with our simulated data. We find that a (quantitatively) crucial aspect in the formulation of these density functional theories is that they recognize that end monomers exclude more volume to the surrounding, than inner ones do.

II. MODEL AND SIMULATIONS

The simulations are performed in two different ensembles GCE and IE, described in more detail below. For every configuration, N polymers with r monomers per chain are confined between two planar infinite surfaces, separated by a distance h, in a parallel arrangement,. The simulation box has a side length L and a surface area $S=L^2$. The monomers are modeled as hard spheres of diameter σ. These are connected with rigid bonds, of length σ, forming a pearl-necklace polymer. This is illustrated in Fig. 1. Intrinsic chain stiffness is introduced via a bend parameter ϵ. The bond angle potential between two consecutive bonds along the chain, i and $i+1$, is given by

$$\beta E_B(i,i+1) = \epsilon(1-\cos\,\theta_{i,i+1}), \tag{1}$$

where θ is the angle between the bond vectors and β is the inverse thermal energy. A positive value of ϵ tends to stretch the chain. The polymer configurations were sampled efficiently by a combination of three different Monte Carlo steps: translation of the whole polymer, reptation, and crankshaft moves. In a standard reptation step, a trial configuration is generated by randomly choosing an end monomer and attaching it, at any angle, to the other end of the polymer. With a bond angle potential it is advantageous to sample the new angle from a Boltzmann distribution, with a weight given by the value of E_B [28]. In GCE simulations, internal configurations of chains are also sampled by the gradual buildup of polymers, via the addition step. Periodic boundary conditions are applied in the directions (x,y) parallel to the surfaces. The monomers interact with the surfaces via a soft monomer-surface potential:

$$V(z,h) = w(z) + w(h-z), \tag{2}$$

where $w(z)$ is modeled as

$$\beta w(z) = Ae^{-z/\sigma}\left[\left(\frac{\sigma}{z}\right)^6 - \left(\frac{\sigma}{z}\right)^3\right], \tag{3}$$

where z is the distance from the left surface. The parameter A is in this work set to 25, which results in a maximum attraction of around $-1.84kT$, located at approximately 1.2σ from the surface. Note that this adsorption potential decays rather rapidly due to the presence of an exponential factor. In this work, both attractive and repulsive monomer-surface interaction potentials have been studied. The repulsive surface is modeled by removing the attractive term on the right-hand side of Eq. (3).

A. Isotension ensemble

The natural thermodynamic potential for a canonical ensemble of N polymers at temperature T confined in a slit of separation h with a surface area S is the Helmholtz free energy $A(N,S,T,h)$. It is an extensive function of both N and S, which gives

$$A = \mu N - P_{\parallel}Sh, \tag{4}$$

where μ is the chemical potential and T is the temperature. The pressure acting parallel to the surfaces, $P_{\parallel}$, is defined as

$$P_{\parallel} = -\frac{1}{h}\left(\frac{\partial A}{\partial S}\right)_{T,N,h}. \tag{5}$$

In isotension ensemble simulations, the surface area is allowed to fluctuate. These fluctuations are stabilized by the parallel pressure, which is an input parameter chosen *a priori*. The partition function Q is given by

$$Q(h,N,P_{\parallel},T) = \frac{h}{\Lambda^{3N}N!}\int_0^{\infty} e^{-\beta P_{\parallel}Sh}dS \times \int e^{(-\beta U[\mathbf{r}_1^1,\ldots,\mathbf{r}_r^N])}d\mathbf{r}_1^1,\ldots,d\mathbf{r}_r^N. \tag{6}$$

U is the interaction part of the Hamiltonian, which is a function of the monomer coordinates $\{\mathbf{r}_1^1,\ldots,\mathbf{r}_r^N\}$. $\mathbf{r}_i^l$ is the position of the ith monomer in the lth polymer. Area fluctuations

from S_0 to S_1 in the simulations are accomplished by rescaling the coordinates $x_{c.m.}$ and $y_{c.m.}$ of all centers of mass of the polymers:

$$(x_{c.m.},y_{c.m.}) \rightarrow \lambda(x_{c.m.},y_{c.m.}), \tag{7}$$

where

$$\lambda = \sqrt{\frac{S_1}{S_0}}. \tag{8}$$

The monomer (x-y) coordinates of each chain are then translated in the following way:

$$x' = x + x_{c.m.}(\lambda - 1),$$

$$y' = y + y_{c.m.}(\lambda - 1). \tag{9}$$

Changes in the area S by an amount ΔS $(S_0 - S_1)$ are accepted with a probability

$$\mathrm{acc}(S_0 \rightarrow S_1) = \min[1, e^{[-\beta P_\parallel h \Delta S + N \ln(S_1/S_0) - \beta \Delta U]}], \tag{10}$$

where

$$\Delta U = U[\mathbf{r}_1^{1'}, \ldots, \mathbf{r}_r^{N'}] - U[\mathbf{r}_1^1, \ldots, \mathbf{r}_r^N]. \tag{11}$$

The area fluctuations are quite time consuming, since a recalculation of the total energy of the system is required. In our simulations, they constituted one percent of the total number of Monte Carlo moves.

1. Free-energy difference method

In order conserve the chemical potential when changing the surface separation, the ratio of the partition functions $Q(h_i)$ and $Q(h_j)$ for any two separations h_i and h_j should be unity:

$$\frac{Q(h_i)}{Q(h_j)} = 1. \tag{12}$$

In order to achieve this, we have employed an optimized version of the FEDM [19,20]. The theory successfully couples the change in separation with a proper adjustment of the parallel pressure. By a virtual transverse scaling of the center-of-mass coordinates ($z_{c.m.}$) of system h_0 and a concomitant translation of the monomer coordinates, the perturbation energy ΔU is obtained and the following energy function is sampled:

$$e(S,h_0,h_1) = \langle e^{-\beta \Delta U(h_0,h_1)} \rangle_{h_0,S}. \tag{13}$$

This quantity, as well as the surface probability distribution $f(S,h_0)$, can be tabulated as a discrete function of S. Equation (12) can be rewritten as

$$\frac{Q(h_1)}{Q(h_0)} = \left(\frac{h_1}{h_0}\right)^{N+1} \int_0^\infty f(S,h_0) e(S,h_0,h_1) \times e^{\{-\beta S[P_\parallel(h_1)h_1 - P_\parallel(h_0)h_0]\}} dS = 1. \tag{14}$$

For a rigorous derivation, see Ref. [19]. Subsequent to a simulation at a reference separation h_0 with a lateral pressure $P_\parallel(h_0)$, Eq. (14) is solved iteratively until $P_\parallel(h_1)$ has been found. This pressure is then used to take the next step in h.

2. Optimizing the FEDM

The FEDM only uses the information obtained by sampling the h_0 distribution. The accuracy of the free-energy estimate will decrease with increasing $|h_1 - h_0|$ because of the diminishing overlap between the ensembles. However, the efficiency can be enhanced considerably by collecting data from two overlapping ensembles [22,29]. In this work, this is done by using an IE-adapted version of Bennett's optimized rate method, developed by Forsman and Woodward [30]. The variance of the free-energy difference between two overlapping ensembles is minimized, which increases the efficiency of the simulations with about an order of magnitude. For the present model system, employing this method is even more crucial, since the FEDM cannot be used to predict the equilibrium pressure at a *larger* separation in a model system containing rigid bonds. The reason is that the FEDM scheme in these cases fails to sample the complete configuration space at the larger separation.

The starting point of optimizing the FEDM is to write a general formula for the ratio of the partition functions at h_0 and h_1. Note that the configuration spaces of the two macrostates at h_0 and h_1 are congruent because of trivial scaling of the coordinates in the perturbation scheme:

$$\frac{Q_{h_1}}{Q_{h_0}} = \frac{Q_{h_1} \int\int W e^{-\beta(H_1+H_0)} dq^N dS}{Q_{h_0} \int\int W e^{-\beta(H_0+H_1)} dq^N dS} = \frac{\langle W e^{-\beta H_1} \rangle_{h_0}}{\langle W e^{-\beta H_0} \rangle_{h_1}}. \tag{15}$$

The weight function $W = W(\mathbf{q}^N, S)$ is an everywhere-finite function of the coordinates and $\beta H_i = \beta[U(\mathbf{q}^N, h_i, S) + P_\parallel(h_i) S h_i] - (N+1) \ln h_i$. The idea is to choose the weight function as the one that minimizes the variance of the free energy difference, $\beta \Delta G = \ln Q_{h_1} - \ln Q_{h_0}$. The optimal weight is [21]

$$W = \frac{c}{Q(h_1)e^{-\beta H_0} + Q(h_0)e^{-\beta H_1}}, \tag{16}$$

where c is a constant. After insertion of the optimized expression for W in Eq. (15) and some algebraic manipulations, we get the following expression for the quotient between $Q(H_1)$ and $Q(H_0)$ [21]:

$$\frac{Q(h_1)}{Q(h_0)} = \left[\frac{\int_0^\infty \int_{-\infty}^\infty f(S,h_0) \rho_0(\Delta U, S) \mathcal{F}(H_0 - H_1 + C) d\Delta U dS}{\int_0^\infty \int_{-\infty}^\infty f(S,h_1) \rho_1(\Delta U, S) \mathcal{F}(H_1 - H_0 - C) d\Delta U dS} \right]^{0.5}, \tag{17}$$

where $\mathcal{F}$ is the Fermi function, $\mathcal{F}(x) = 1/(1+e^x)$, and

$$C = \ln\left[\frac{Q(h_1)}{Q(h_0)}\right]. \tag{18}$$

ρ_0 is a conditional probability that the system at h_0 has an energy difference $\Delta U = U(h_1) - U(h_0)$ at a given area S. By virtual transitions from h_0 to h_1, we map the system at h_1 and $\rho_0(\Delta U, S)$ is being tabulated. A simulation at h_1 maps the h_0 system, and $\rho_1(\Delta U, S)$ is obtained.

In this work, the FEDM was used to predict the parallel pressure at h_1. Let us denote this pressure $P_\parallel^0(h_1)$. With Bennett's method we try to find the reversible path between the two systems by mapping the h_0 system through virtual jumps from the h_1 space. The aim is to correct $P_\parallel^0(h_1)$, obtained from the FEDM. The corrected pressure is denoted $P_\parallel(h_1)$. As a consequence of the incorrect FEDM pressure obtained at h_1, also a slightly incorrect area probability density denoted $f^0(S,h_1)$ is sampled throughout the simulation. The correct area probability density $f(S,h_1)$ can nevertheless be computed with the following perturbation expression:

$$f(S,h_1) = \frac{f^0(S,h_1)e^{-\beta[P_\parallel(h_1)-P_\parallel^0(h_1)]hS}}{\int_0^\infty f^0(S,h_1)e^{-\beta[P_\parallel(h_1)-P_\parallel^0(h_1)]hS}dS}. \tag{19}$$

Remembering that $Q(h_0)$ is equal to $Q(h_1)$ at equilibrium, the constant in Eq. (17) will be zero.

If we recalculate the pressure-corrected area probability distribution in our optimization scheme iteratively by varying $P_\parallel(h_1)$ until the right-hand side of the expression in Eq. (17) equals 1, a near-optimal value for $P_\parallel(h_1)$ is found [22,31]. In this paper, successive FEDM predictions of the parallel pressure, corrected by Bennett's method, were used to generate the equilibrium parallel pressure as a function of surface-surface separation. When $h(i+1) > h(i)$, the mapping of the $h(i+1)$ space, using only one ensemble, is wrong for the case with hard-sphere monomers and rigid bonds. Some parts of the configuration space become inaccessible, and the FEDM completely fails to work. This is not the case with Bennett's method, which is correct in both directions. The results presented in this work have been obtained by stepping upwards and downwards from a reference separation intermediate to the initial and final separations. In fact, Bennett's method is so efficient that the FEDM is rarely needed at all. It is sufficient to use a constant initial value of pressure as a guess for the pressure at all separations.

3. Calculating the parallel and osmotic pressure

The surface interactions are conveniently characterized by the free energy per unit area, g_s. At equilibrium, g_s is related to the bulk pressure P_b and the parallel pressure $P_\parallel$ [32]:

$$g_s = [P_b - P_\parallel(h)]h. \tag{20}$$

The quantity $-P_\parallel h$ is the grand potential per unit area and is obtained directly in an IE simulation (subsequent to the Bennett correction). From Eq. (4), we see that the osmotic pressure at equilibrium, $P_\perp$, can be calculated as

$$P_\perp = \frac{d(P_\parallel(h)h)}{dh}. \tag{21}$$

P_b is estimated from large surface-surface separations.

The internal osmotic pressure could also be obtained from the average force. At equilibrium, the derivative of the logarithm of the IE partition function with respect to the separation is zero. Denoting the canonical configurational integral by Z, we can write the IE partition function as

$$Q(h,N,P_\parallel,T) = \frac{h}{\Lambda^{3N}N!}\int_0^\infty Z\, e^{-\beta P_\parallel Sh}dS, \tag{22}$$

where

$$Z \equiv \int e^{(-\beta U[\mathbf{r}_1^1,\ldots,\mathbf{r}_r^{N_r}])}d\mathbf{r}_1^1,\ldots,d\mathbf{r}_r^N. \tag{23}$$

This leads to

$$\frac{1}{h} + \frac{\beta h}{N!}\left(\frac{\int_0^\infty \left(\frac{\partial \ln Z}{\partial h}\right) Z\, e^{-\beta P_\parallel Sh}dS}{Q}\right. \tag{24}$$

$$\left. - \frac{\int_0^\infty Z\, S\left(\frac{\partial P_\parallel h}{\partial h}\right) e^{-\beta P_\parallel Sh}dS}{Q}\right) = 0. \tag{25}$$

Using Eq. (21), we can write the above expression as

$$P_\perp = \frac{\partial P_\parallel h}{\partial h} = \frac{1}{\beta h\langle S\rangle} + \frac{\langle F\rangle}{\langle S\rangle}, \tag{26}$$

where F is the total force normal to the surfaces.

B. Grand canonical ensemble

Chemical equilibrium in an open system can also be maintained in a grand canonical ensemble. The probability of successful insertions or deletions of an entire chain is in the conventional GCE very small. A method to circumvent this problem was first introduced by Rosenbluth and Rosenbluth in 1955 [11]. With their approach, the number of trial insertions of a chain in a region of high acceptance probability is enhanced. This bias has to be taken into account, and the correct acceptance rule for the insertion of a chain reads

$$\mathrm{acc}(N \to N+1) = \min\left[1, W_{N+1}\frac{Ve^{\beta\mu}}{N+1}\right]. \tag{27}$$

W_{N+1} is the Rosenbluth factor for inserting a chain. It is determined by the following procedure: a number k of trial insertion coordinates for the first monomer in the chain are randomly generated in the simulation box. For each position, the Boltzmann factor $e^{-\beta U_i}$ is calculated, where U_i is the change of the potential energy of the system, due to a virtual insertion of monomer i. One of the coordinates is then being selected with a probability

$$P_i = \frac{e^{-\beta U_i}}{w_i}, \tag{28}$$

where

$$w_i = \sum_{j=1}^{k} e^{-\beta U_j}. \tag{29}$$

This coordinate constitute the position of the first monomer of the trial chain conformation. The position of the next monomer, $i+1$, is generated from a set of k trial coordinates separated a bond length from monomer i. For flexible chains, coordinates evenly distributed on a sphere centered at (x_i, y_i, z_i) would suffice. But with a bond angle potential, it is advantageous to sample the new angle from a Boltzmann distribution, with a weight given by the value of E_B [28]; see Eq. (1). When the whole trial chain of r monomers has been built up, the Rosenbluth factor is calculated:

$$W_{N+1} = \prod_{i=1}^{r} \frac{w_i}{k}. \tag{30}$$

From the Rosenbluth factor the total chemical potential μ can be calculated as

$$\beta\mu = -\left[\ln W_{N+1} + \ln\left(\frac{V}{N+1}\right)\right]. \tag{31}$$

The procedure for deleting a chain is as follows: Choose an existing chain in the system and calculate $k-1$ number of trial positions around each monomer. The kth position is that of the already existing monomer. Then the Rosenbluth factor is calculated as in Eq. (30).

The osmotic pressure in the GCE was calculated from a virial expression similar to that in Eq. (26), excluding the first term, which is a consequence of the IE. To obtain free energies from GCE results, the osmotic pressure curve was splined and the bulk pressure was subtracted. The resulting net pressure curve was then numerically integrated according to Eq. (32):

$$g_s(h) = \int_h^\infty [P_\perp(h') - P_b]dh'. \tag{32}$$

At large surface separations, g_s approaches twice the tension at a single surface, γ_s. The net surface interaction per unit area is conveniently expressed in terms of $\Delta g_s(h) \equiv g_s(h) - 2\gamma_s$. We define $P \equiv P_\perp - P_b$ as the net osmotic pressure.

C. Density functional theory

The theory is based on Woodward's polymer density functional formalism [27], although we shall adopt the more refined versions for flexible [33] and semiflexible [34] chains, introduced in subsequent work. We will also exploit a few previously untested versions.

Denoting the coordinate of the ith monomer by $\mathbf{r}_i$, we can write the full configuration of an r-mer as $\mathbf{R} = (\mathbf{r}_1, \ldots, \mathbf{r}_r)$. The bond potential V_B connecting neighboring monomers will in our pearl-necklace model fulfill $e^{-\beta V_B(\mathbf{R})} \propto \Pi_{i=1}^{r-1} \delta(|\mathbf{r}_{i+1} - \mathbf{r}_i| - \sigma)$. It is useful to define a density distribution $N(\mathbf{R})$ such that $N(\mathbf{R})d\mathbf{R}$ is the number of polymer molecules having configurations between $\mathbf{R}$ and $\mathbf{R}+d\mathbf{R}$. The monomer density $n(\mathbf{r})$ is obtained from $n(\mathbf{r}) = \int \Sigma_{i=1}^{r} \delta(\mathbf{r} - \mathbf{r}_i) N(\mathbf{R}) d\mathbf{R}$. The free-energy functional $\mathcal{F}[N(\mathbf{R})]$ is generally written as the sum of an ideal ($\mathcal{F}^{id}[N(\mathbf{R})]$) and an excess ($\mathcal{F}^{ex}[N(\mathbf{R})]$) contribution: $\mathcal{F}[N(\mathbf{R})] = \mathcal{F}^{id}[N(\mathbf{R})] + \mathcal{F}^{ex}[N(\mathbf{R})]$. The ideal part has the exact formulation: $\beta\mathcal{F}^{id}[N(\mathbf{R})] = \int N(\mathbf{R})\{\ln[N(\mathbf{R})] - 1\}d\mathbf{R} + \beta \int N(\mathbf{R})[V_B(\mathbf{R}) + V_{ex}(\mathbf{R})]d\mathbf{R}$, where $V_{ex}(\mathbf{R})$ is an external potential, in our case emanating from the surfaces.

Contrary to $\mathcal{F}^{id}[N(\mathbf{R})]$, $\mathcal{F}^{ex}$ has to be approximated. We have investigated several different formulations, which can be partitioned in three separate groups. With formulations of the first kind, the excess contribution has the following structure:

$$\mathcal{F}^{ex}[n(\mathbf{r})] = \int n(\mathbf{r}) f(\bar{n}) d\mathbf{r}, \tag{33}$$

where $\bar{n}$ is a coarse-grained density, while $f(n)$ is the excess free energy per monomer in a bulk solution with a monomer density n. The use of coarse-grained, or weighted, densities was introduced by Nordholm and co-workers [35]. It allows treatment of nonlocal excluded volume effects. There are several different recipes for the evaluation of $\bar{n}(\mathbf{r})$, with the common strategy that it is expressed in terms of weighted contributions from local densities in the vicinity of $\mathbf{r}$:

$$\bar{n}(\mathbf{r}) = \int n(\mathbf{r}') w(|\mathbf{r} - \mathbf{r}'|) d\mathbf{r}'. \tag{34}$$

Sometimes the weighted density is expressed as a sum of such integrals. In most cases, we shall adopt the original recipe, proposed by Nordholm *et al.*:

$$w(r) = \frac{3}{4\pi\sigma^3}\Theta(\sigma - r), \tag{35}$$

where $\Theta(x)$ is the Heaviside step function,

$$\Theta(x) = \begin{cases} 1, & x \le 0, \\ 0, & x > 0. \end{cases}$$

As we shall see, comparisons with results using a more elaborate version proposed by Tarazona and Evans [36], suggest that the specific choice of weighting has little influence on the investigated surface interactions. The excess free energy per monomer, $f(n)$, is conveniently obtained by integration of a polymer equation of state (EOS). Again, there are several different alternatives, and we will compare the following versions.

(i) The "Chiew" EOS, suggested by Chiew [37].

(ii) The "Song" EOS, where Song *et al.* [38] modified the Chiew EOS so as to utilize the Boublik-Mansoori-Carnahan-Starling-Leland (BMCSL) [39,40], rather than the Percus-Yevick [41] expression for the contact value of the radial distribution function.

(iii) The thermodynamic perturbation theory EOS, "TPT1," proposed by Wertheim [42]. Actually, we will adopt a slightly refined version [43], utilizing the BMCLS expression.

Integrating the Chiew EOS for a pure polymer fluid, or a polymer solution with an implicit solvent (the Mcmillan-Mayer approach), leads to

$$\beta f_{Chiew}(n) = \frac{3\eta}{1-\eta}\left(1+\frac{\eta}{2(1-\eta)}\right) - \frac{3(r-1)\eta}{2r(1-\eta)} - \frac{1}{r}\ln[1-\eta], \tag{36}$$

where $\eta = \pi n\sigma^3/6$. Corresponding expressions are

$$\beta f_{Song}(n) = \frac{\eta}{1-\eta}\left(3+\frac{1}{1-\eta}\right) - \frac{(r-1)\eta}{4r(1-\eta)}\left(6+\frac{\eta}{1-\eta}\right) + \left(1-\frac{1}{r}\right)\ln[1-\eta] \tag{37}$$

for the Song EOS and

$$\beta f_{TPT1}(n) = \frac{\eta}{1-\eta}\left(3+\frac{1}{1-\eta}\right) + \frac{1-r}{r} \times \ln\left[\frac{1}{1-\eta} + \frac{3\eta}{(1-\eta)^2} + \frac{\eta^2}{2(1-\eta)^3}\right] \tag{38}$$

for the TPT1 EOS.

The second category of functionals we will investigate differs from the above in one, as we shall demonstrate, quantitatively important aspect. They recognize that end monomers exclude more volume to the surrounding than "inner" ones do and are derived from a dimer fluid reference. The excess part of the functional can in these cases be written

$$\mathcal{F}^{ex}[n(\mathbf{r})] = \int n_c(\mathbf{r}) f_c(\bar{n}) d\mathbf{r} + \int n_e(\mathbf{r}) f_e(\bar{n}) d\mathbf{r}, \tag{39}$$

where $n_e(\mathbf{r})$ is the density of end monomers, while $n_c(\mathbf{r}) = n(\mathbf{r}) - n_e(\mathbf{r})$ is the density of all inner monomers. Two formulations below to this group: the generalized-Flory dimer (GFD) and the TPTD1. We start by a recapitulation of the GFD functional, which is based on an equation of state proposed by Honnell and Hall [44]. By integrating this EOS, Woodward and Yethiraj [33] obtained the following expression:

$$\beta f_{GFD}(n) = \frac{r-2}{r}\frac{v_e(r)-v_e(2)}{v_e(2)-v_e(1)}[a_2(n)-a_1(n)] + \frac{a_2(n)}{r}, \tag{40}$$

where $v_e(r)$ is the volume that an r-mer excludes from its surrounding [45]. We have used the approximations suggested by Wichert *et al.* [46]. Specifically, $v_e(1) = 4\pi\sigma^3/3$, $v_e(2) = 9\sigma^3\pi/4$, and $v_e(3) \approx 9.83\sigma^3$. For $r > 3$, they used the approximation

$$v_e(r) = v_e(3) + (r-3)[v_e(3) - v_e(2)] - 0.04915\sigma^3(r-3)^{1.09}, \tag{41}$$

where the last term is an empirically determined correction. For a pure polymer fluid, the expressions for a_i simplifies to [34]

$$a_1(n) = \frac{1}{1-\eta}\left(2+\frac{1}{1-\eta}\right) - 3 \tag{42}$$

and

$$a_2(n) = \frac{5}{4}\ln[1-\eta] + \frac{9}{4(1-\eta)}\left(1+\frac{1}{1-\eta}\right) - \frac{9}{2}. \tag{43}$$

The GFD version of Eq. (39) reads

$$\beta\mathcal{F}^{ex}[n(\mathbf{r})]_{GFD} = \frac{1}{r-2}\int n_c(\mathbf{r})\frac{v_e(r)-v_e(2)}{v_e(2)-v_e(1)}[a_2(\bar{n}(\mathbf{r})) - a_1(\bar{n}(\mathbf{r}))]d\mathbf{r} + \frac{1}{2}\int n_e(\mathbf{r}) a_2(\bar{n}(\mathbf{r}))d\mathbf{r}. \tag{44}$$

We shall later see that a separate treatment of end monomer volume exclusion improves the accuracy of predicted surface interactions quite considerably. The "end effect" is furthermore significant for surprisingly high degrees of polymerizations. In order to facilitate direct comparisons with a corresponding approach in which the all monomers are treated equally, we will sometimes include predictions from the GFD functional one obtains if the approach suggested in Eq. (33) is used:

$$\beta\mathcal{F}^{ex}[n(\mathbf{r})]_{GFD\text{-}AME} = \frac{1}{r}\int n(\mathbf{r})\frac{v_e(r)-v_e(2)}{v_e(2)-v_e(1)}[a_2(\bar{n}(\mathbf{r})) - a_1(\bar{n}(\mathbf{r}))]d\mathbf{r} + \frac{1}{r}\int n(\mathbf{r}) a_2(\bar{n}(\mathbf{r}))d\mathbf{r}, \tag{45}$$

where the index "AME" signifies an "all monomers equal" excluded volume treatment.

The second EOS in the category that uses a dimer reference fluid is the TPTD1, derived by Chang and Sandler [47]. An integration leads to

$$\beta f_{TPTD1}(n) = \frac{\eta}{(1-\eta)^2}(4-3\eta) - \ln\left[\frac{1-\frac{1}{2}\eta}{(1-\eta)^3}\right] - \frac{1-2/r}{2}\ln\left[\frac{\frac{1}{2}+\eta}{(1-\eta)^2}\right], \tag{46}$$

suggesting that the corresponding excess functional $\mathcal{F}^{ex}[n(\mathbf{r})]_{TPTD1}$ can be written in the form given by Eq. (39), with

$$f_c(n) = \frac{\eta}{(1-\eta)^2}(4-3\eta) - \ln\left[\frac{1-\frac{1}{2}\eta}{(1-\eta)^3}\right] - \frac{1}{2}\ln\left[\frac{\frac{1}{2}+\eta}{(1-\eta)^2}\right] \tag{47}$$

and

$$f_e(n) = \frac{\eta}{(1-\eta)^2}(4-3\eta) - \ln\left[\frac{1-\frac{1}{2}\eta}{(1-\eta)^3}\right]. \tag{48}$$

In other words, this functional also takes into account that end monomers exclude more volume than central ones do. A corresponding functional, in which all monomers are treated equally, can be constructed in the same manner as we did with the GFD. It serves as a useful reference and will be denoted TPTD1-AME.

The last of our tested functionals in this work belongs to a third category. It is fundamentally different from the other functionals, since it does not rely on an EOS, or at least not an "ordinary" one. Instead, the functional is based on what we call the "locally incompressible fluid" approach (LIF). It is essentially a continuum version of the Scheutjens-Fleer theory [48] and was first introduced by Forsman *et al.* [49]. The main assumption is that the fluid, including the solvent, is *locally* incompressible. This is formulated by the following constraint: $n_s(z)+n(z)=n_0$, where n_0 is the fixed total density, while n_s is the density of an implicit solvent. Hence, in analogy with the Flory-Huggins, or Scheutjens-Fleer, theories, the solvent merely "fill up" empty space. This local incompressibility constraint implies that we impose an excess free energy that is constant as long as the constraint is fulfilled and infinite otherwise. In accordance with the lattice theory of Scheutjens and Fleer, we shall let n_0 correspond to cubic close packing—i.e., $n_0\sigma^3=1$. It should be pointed out that predictions by this functional hardly can be expected to agree quantitatively with continuum simulations, since the latter implicitly assumes *global* incompressibility (via McMillan-Mayer theory, connecting osmotic pressure with solvent chemical potential).

Having chosen a suitable approximation for $\mathcal{F}^{ex}$, the grand potential $\Omega=-P_{\|}h$ is obtained from

$$\Omega[N(\mathbf{R})] = \mathcal{F}^{id}[N(\mathbf{R})] + \mathcal{F}^{ex}[N(\mathbf{R})] - \mu_p \int N(\mathbf{R})d\mathbf{R}, \tag{49}$$

where μ_p is the bulk polymer chemical potential. The interaction free energy per unit area, $g_s(h)$, is given by $g_s(h)=\Omega_{eq}/S+P_bh$ where Ω_{eq} is the equilibrium grand potential and S is the surface area. The functional is simplified by integration over the (x,y) plane parallel to the surfaces; i.e., we neglect lateral heterogeneities [50].

With the LIF approach, we get

$$\beta\Omega[N(\mathbf{R})] = \beta\mathcal{F}^{id}[N(\mathbf{R})] + \int \{n_0 - n(z)\}\{\ln[n_0 - n(z)] - 1\}dz + \beta\mathcal{F}^{ex} + \int \beta\{V_{ex}(z) - \mu_p\}n(z)dz - \int \beta\mu_s\{n_0 - n(z)\}dz, \tag{50}$$

where $\mathcal{F}^{ex}$ is a functional of the local total density and μ_s is the chemical potential of the solvent. Remember that the total density is constrained to be constant; i.e., $\mathcal{F}^{ex}$ is constant. Hence, the free energy can be considered a functional of the monomer density only and thus describes an *effective* one-component polymer fluid. Note also that it is implicitly assumed that the external potential V_{ex} acts on the monomers only, since only "excess" quantities matter in a local incompressibility approach. The solvent particles are confined by an imaginary hard wall, which we have located 0.75σ from the surface, which is close enough for the monomer density to have decayed to an insignificant value.

1. Semiflexible polymers

As mentioned previously, semiflexible chains are modeled via a "stiffness potential" E_B. With $\mathbf{s}_i$ denoting the bond vector between monomers i and $i+1$, we can rewrite Eq. (1) as $\beta E_B=\epsilon\left(1-\frac{\mathbf{s}_i\cdot\mathbf{s}_{i+1}}{\sigma^2}\right)$. A more intuitive feeling for the role played by the stiffness parameter ϵ is obtained by noting that, if we neglect hard-core effects, the polymer persistence length $\xi_p=\langle\mathbf{R}_{ee}\cdot\mathbf{s}_1/\sigma\rangle$ is given by

$$\xi_p/\sigma = \frac{\epsilon(1-e^{-2\epsilon})}{1-e^{-2\epsilon}(1+2\epsilon)}, \tag{51}$$

where $\mathbf{R}_{ee}$ is the position vector between the end monomers. Thus, even for moderate values of ϵ, $\xi_p/\sigma\approx\epsilon$. Integrating the Boltzmann factor $\exp(-\beta E_B)$ across the (x,y) plane leads to

$$\Psi(\Delta z_i,\Delta z_{i+1}) = e^{\epsilon(1-\Delta z_i\Delta z_{i+1}/\sigma^2)} I_0\left\{\epsilon\left[1-\left(\frac{\Delta z_i}{\sigma}\right)^2\right]^{1/2} \times\left[1-\left(\frac{\Delta z_{i+1}}{\sigma}\right)^2\right]^{1/2}\right\}, \tag{52}$$

where $I_0(x)=\frac{1}{2\pi}\int_0^{2\pi}\exp[-x\cos\Phi]d\Phi$ is a modified Bessel function and $\Delta z_i\equiv z_{i+1}-z_i$. Minimizing the free-energy functional for semiflexible chains of hard-sphere monomers confined by surfaces gives the following expression for the equilibrium monomer density profile:

$$n(z) = e^{\beta\mu_p}\sum_{i=1}^{r}\int_0^h \delta(z-z_i)\prod_{j=1}^{r} e^{-\Lambda(z_j)}\prod_{k=1}^{r-1}\Theta(|\Delta z_k|-\sigma) \times\prod_{l=1}^{r-2}\Psi(\Delta z_l,\Delta z_{l+1})dz_1\cdots dz_r, \tag{53}$$

where $\Lambda(z)=\beta[\delta\mathcal{F}_{ex}/\delta n(z)+V_{ex}(z)]$. In order to simplify the notation, we here have assumed that $\mathcal{F}_{ex}$ does not discriminate between end monomers and central ones. The generali-

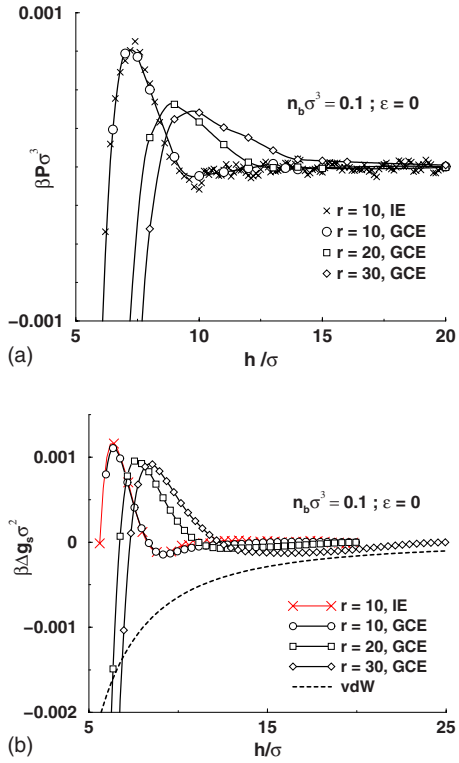

FIG. 2. (Color online) (a) Net osmotic pressure curves as a function of separation in solutions containing flexible polymers (ϵ =0) of various chain lengths. The surfaces are repulsive, and $n_b\sigma^3$=0.1. (b) Free energy of interaction per unit surface area for the system in (a), obtained as described in the text above. The dashed line corresponds to a van der Waals interaction with a Hamaker constant of 10^{-20} J.

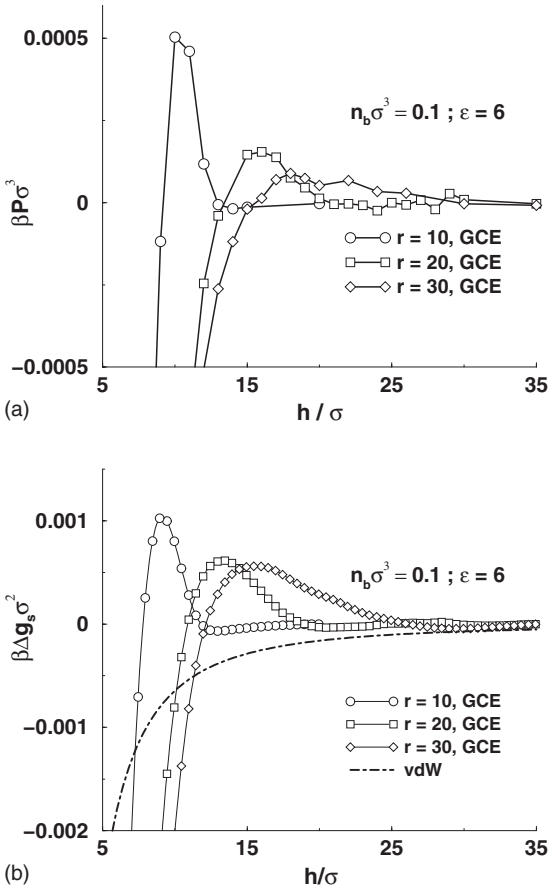

FIG. 3. (a) Net osmotic pressure curves as a function of separation in the presence of semiflexible polymers (ϵ=6) of various chain lengths. The surfaces are repulsive, and $n_b\sigma^3$=0.1. (b) Free energy of interaction per unit surface area for the system in graph (a).

zation to such cases is straightforward. Equation (53) is easily solved by iteration using a propagator approach.

III. RESULTS

A. Repulsive surfaces

Results for polymers confined between monomer repelling surfaces were obtained using GCE simulations. The choice of simulation ensemble (GCE or IE) depends on the accuracy with which the osmotic pressure in the slit can be determined. In the case with repulsive surfaces, we found that GCE simulations are preferable, at least for such short chains. GCE simulations have the added advantage that surface force computations can be trivially "parallelized." In Fig. 2(a) we display the net osmotic pressure at various surface separations, as obtained in the presence of flexible chains. The bulk monomer density was set to $n_b\sigma^3$=0.1 by calculating the polymer chemical potential [see Eq. (31)] in a separate bulk simulation. The trend is clear: longer chains generate a more long-ranged repulsive osmotic pressure. Note also the slightly oscillatory behavior observed with the shortest chains. A comparison with an IE simulation for r =10 is included in Fig. 2. As expected the two approaches agree well. In Fig. 2(b), the corresponding free-energy interaction is presented together with a typical van der Waals (vdW) interaction, choosing a Hamaker constant of 10^{-20} J. We see that the sum of the vdW interaction and the polymer-mediated interactions is negative for most separations; i.e., no significant stabilization is created from a solution of flexible polymers, at this particular bulk monomer density.

Figures 3(a) and 3(b) show net osmotic pressures and free energies, respectively, as a function of separation in the presence of semiflexible polymers, ϵ=6. The range of surface-surface interactions increases with the intrinsic rigidity of the dissolved chains. For ϵ=6, this leads to the development of a free-energy barrier exceeding our reference vdW attraction. This is an demonstration of the experimentally well-established phenomenon called "depletion stabilization."

B. Attractive surfaces

Forces between adsorbing surfaces were investigated with IE simulations. The precision obtained from GCE simulations was insufficient, especially with stiff chains. It is also worth noting that a considerably higher precision of the osmotic pressure was obtained with Eq. (21), as compared to the virial expression in Eq. (26). The osmotic pressure was therefore calculated using Eq. (21), and the free-energy

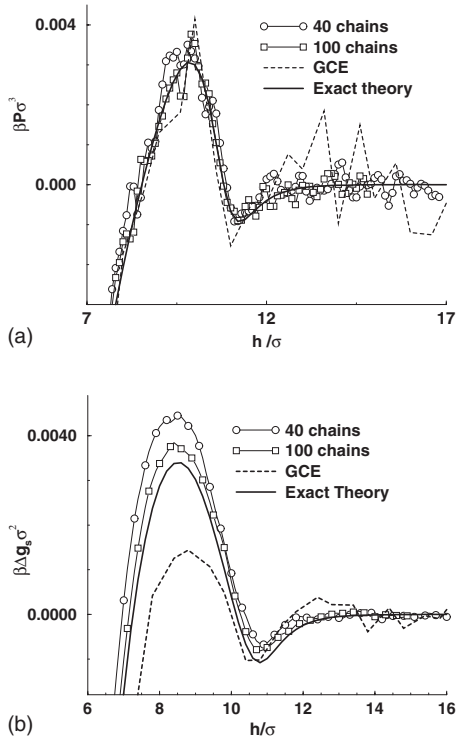

FIG. 4. Interactions between surfaces immersed in a solution of ideal semiflexible decamers, with $\epsilon=14$. Results using the GCE and IE approaches, respectively, are displayed. (a) Net osmotic pressures. (b) Net interaction free energies.

curves were constructed with Eq. (20). In Fig. 4, we explicitly compare the IE and GCE approaches for a system containing ideal semi-flexible polymers ($r=10$ and $\epsilon=14$). To summarize, the problem with the GCE is twofold: First, it is difficult, even with the weighting scheme, to find attractive configurations. This is particularly difficult for stiff chains with hard cores, but the problem as such is general. Second, it becomes very CPU demanding (long simulations) to determine the monomer-wall pressure with satisfactory accuracy, when the surfaces are strongly adsorbing.

The total CPU time spent to span a given separation regime is roughly the same with both approaches. The IE simulations perform considerably better than the GCE simulations. This is particularly evident from the free-energy curves in Fig. 4(b), where the IE results are closer to the exact solution. In fact, the GCE results can differ from the exact curve with as much as 50%. Two different system sizes (40 and 100 polymers) were simulated in the IE. The number of chains in the GCE fluctuated around 40. In graph 4(b), we see that there is a significant size dependence. However, size effects are not nearly as pronounced in a system of interacting chains. This is obvious from the results displayed in Fig. 5, where we compare results from simulations using 16 and 36 hard-sphere polymers, respectively. Because of the small observed differences in these systems, we decided to carry out most simulations with 24 chains.

In Fig. 6, we show surface interactions at three different bulk monomer densities. The chains are semiflexible with $\epsilon=11$. The average end-to-end distance is about 90% of the

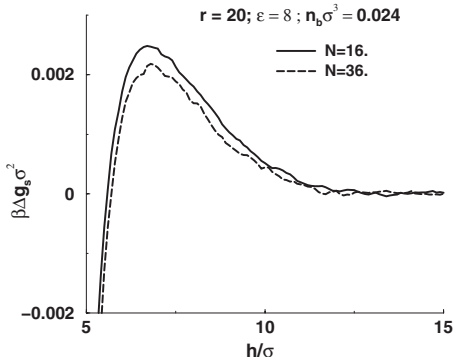

FIG. 5. Size effects in the IE method for a system of hard-sphere polymers. The surfaces are adsorbing. Results from simulations with 16 and 36 chains are compared.

maximum value. Such stiff chains adsorb very strongly, almost saturating the surfaces, and the interaction between the surfaces is then mainly governed by the remaining free chains. At higher concentrations, a depletion interaction dominates at long range. This is caused by nonadsorbed chains being expelled from the slit as the separation is reduced. At such high concentrations, the surfaces are even more saturated by adsorbed chains. This tends to increase the influence of "free" polymers on the surface force [51,52]. At shorter separations, all three curves display a free-energy barrier. This barrier is caused by overlap between the outer parts of the adsorbed layers. At even shorter distances bridging attraction is prevalent and brings the surfaces together. At very short distances a strong repulsive interaction due to overlap between the adsorbed layers determines the overall shape of the interaction curves (not shown).

The inset of Fig. 6(a) highlights the problem of using the virial expression, Eq. (26), to determine the osmotic pressure. The noise reduces substantially when Eq. (21) is used instead. In order to obtain a free-energy curve that resolves both depletion attraction and the repulsive barrier, we had to use the IE approach. In fact, the GCE method, where the pressure must be evaluated with Eq. (26), can give qualitatively wrong results for stiff chains and strong adsorption potentials. The acceptance of inserting and deleting a chain near the surfaces is very low in these cases. Furthermore, even in a canonical simulation, the osmotic pressure is difficult to measure with the virial equation. In summary, the GCE approach suffers from two problems when the chains are stiff and the surfaces are strongly adsorbing: it is computationally demanding to establish the equilibrium density, and the osmotic pressure is poorly estimated with the virial equation. These problems are avoided in the IE with its fixed number of chains and the possibility to use the superior equation (21) to calculate the osmotic pressure.

The effect of varying the intrinsic chain stiffness at different bulk densities is illustrated in Fig. 7. Bulk monomer densities were estimated from the osmotic pressures at large separations. A typical vdW interaction has been added to each graph. Fig. 7(a) shows the cases $\epsilon=8$ and 11 at $n_b\sigma^3=0.029$ and 0.028, respectively. Increasing the stiffness makes the repulsive interaction stronger and more long ranged, implying the possibility of a stronger colloid disper-

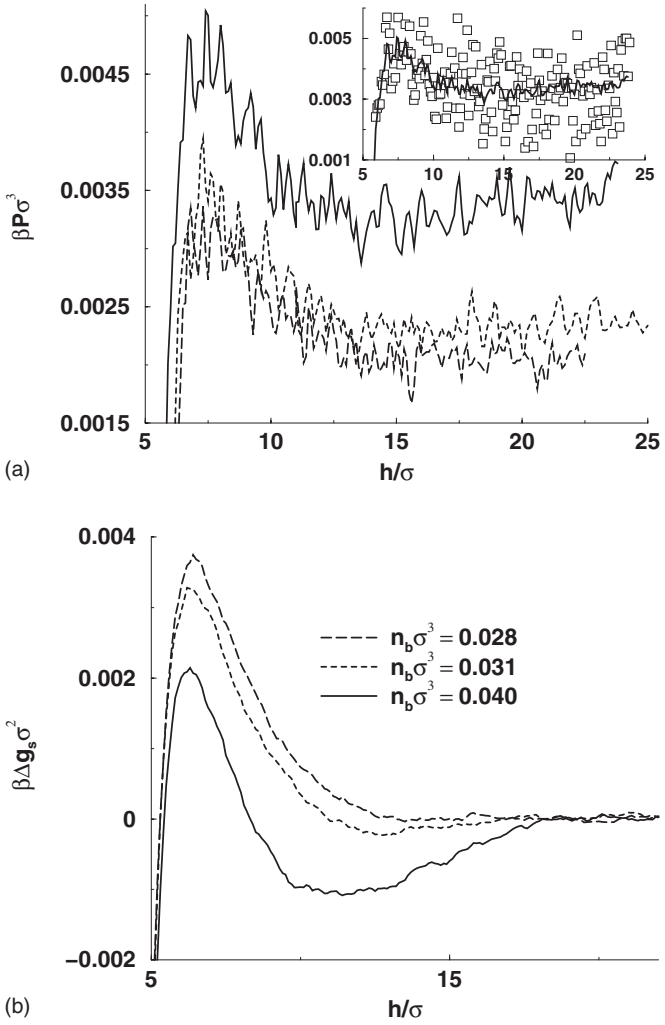

FIG. 6. (a) Net osmotic pressures obtained from Eq. (21) for three various bulk monomer densities of a 20-mer with $\epsilon=11$. $n_b\sigma^3=0.028$ (long-dashed line), $n_b\sigma^3=0.031$ (dashed line), and $n_b\sigma^3=0.040$ (solid line). The squares in the inset show the pressure calculated using the virial equation [Eq. (26)] for $n_b\sigma^3=0.040$. The surfaces are attractive. (b) Net free energy of interaction per surface area for the system in graph (a).

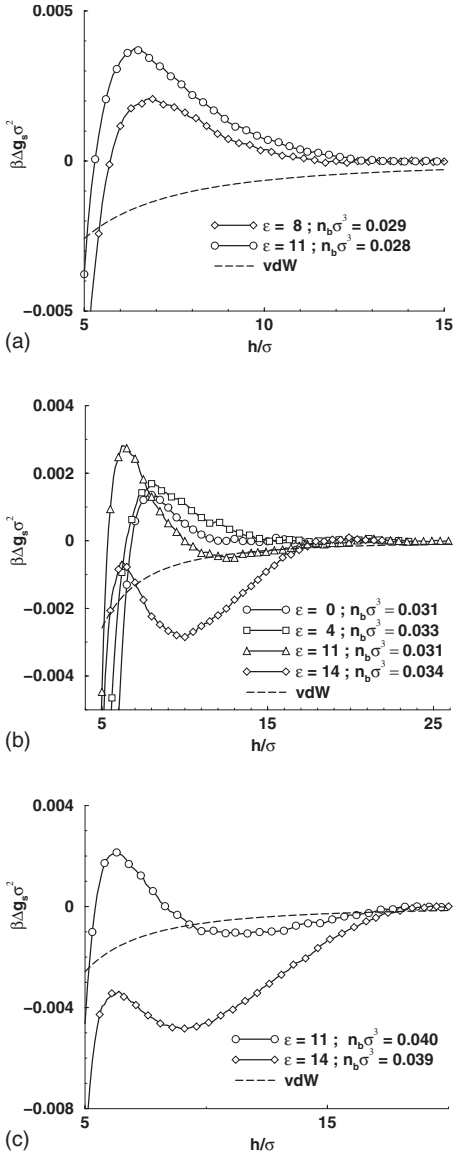

FIG. 7. Free energy per surface area as a function of intrinsic chain stiffness. The graphs are grouped into three different bulk density regimes. The surfaces are attractive and $r=20$.

sion stabilization. In Fig. 7(b), the response of surface interactions to changes of the intrinsic polymer stiffness is shown, at a roughly constant bulk monomer density. Interestingly, the interaction is not a monotonic function of the stiffness. Starting from the fully flexible chain, stiffening it to $\epsilon=4$, renders the barrier higher and more long ranged. Increasing it further, to $\epsilon=11$, shifts the position of the maximum of the barrier to a shorter separation. At the same time, a long-ranged attractive regime starts to form. Increasing the stiffness even further, to $\epsilon=14$, almost completely removes the repulsive barrier. Instead the long-ranged attractive depletion regime dominates. In the extreme limit that the chain is an infinitely stiff rod, the barrier at short range is replaced by a weaker, but more long-ranged, one [52]. The increased range of the depletion interaction for the stiffest chains is related to surface saturation effects, combined with an increased radius of gyration. The probability for stiff chains, stretching out in the solution between the surfaces, is small, due to high cooperativity of monomer adsorption. The surface becomes nearly saturated with polymers, and the depletion interaction dominates at large separations. These saturation effects are more pronounced at higher monomer concentrations, as illustrated in Fig. 7(c).

Extremely stiff chains with a rodlike rigidity are known to display orientational ordering at adsorbing surfaces. We have not found any clear *transition* to ordered phases at the surfaces, but the stiffest athermal chains do display a slight orientational ordering at the surfaces. As was discussed more thoroughly in a previous publication [52], this ordering actually has little influence on the surface interactions.

Figure 8 shows two of the curves in Fig. 7(b) on a different scale, highlighting the remarkable precision of the simulated free-energy barriers. Simulation results of surface interactions are typically displayed on a scale similar to that

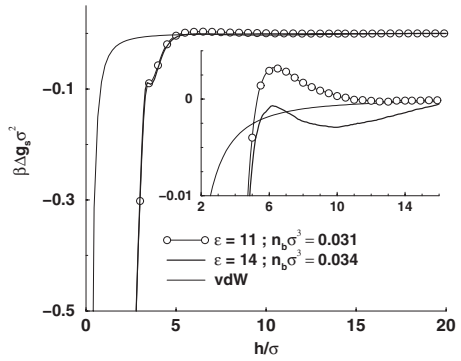

FIG. 8. Two of the curves in Fig. 7(b) ($\epsilon = 11$ and 14), together with a typical vdW interaction. The inset is a magnification around 6σ and reveals the relevant free-energy barriers.

given in the main graph of Fig. 8. Here, the barrier found with the less rigid chains is not discernable. In fact, on this scale, the GCE approach is probably satisfactory (not checked). Note, however, that even if the barrier is small on this scale, it is still comparable to a typical van der Waals attraction and also comparable to surface forces typically measured with SFA or AFM instruments. The inset displays a magnified portion of the graph, where we see how the accuracy and precision of the IE+Bennett approach permits us to evaluate the role of intrinsic chain stiffness. Strong bridging attractions completely dominate at separations between 2σ and 3.5σ. At about 3.5σ there is a small bump in the free energy, which originates from steric restrictions of the confined chains in the slit.

We conclude this section by presenting, in Fig. 9, simulated (IE) interactions between strongly adsorbing surfaces, mediated by flexible and semiflexible 30-mers. When the intrinsic stiffness of the dissolved chains increases from flexible to moderately stiff, the free-energy barrier becomes larger, in agreement with what we have seen for shorter chains. The simulated time per point for the stiff polymer in Fig. 9 was about 7.5 h. With 160 points, the total CPU time amounts to about 50 days. Nevertheless, corresponding GCE simulations would require a substantially increased computational effort and would in practice be almost impossible to run.

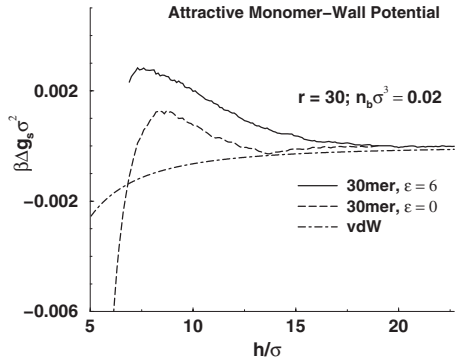

FIG. 9. Free energy of interaction per surface area as a function of the slit width. The system contains 30-mers. $n_b\sigma^3 = 0.022$.

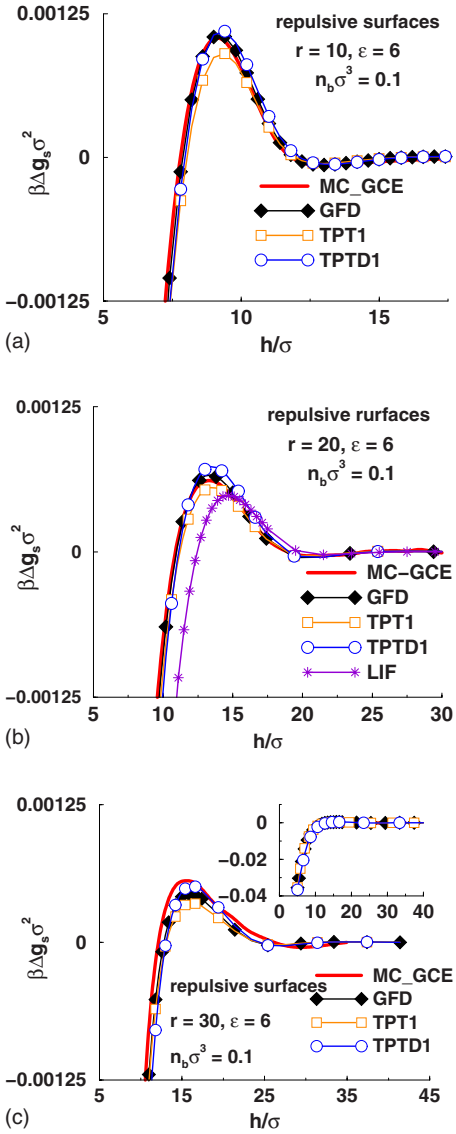

FIG. 10. (Color online) Comparisons between density functional predictions and simulated data of the interaction between repulsive surfaces in the presence of semiflexible (ϵ=6) hard-sphere polymers at a bulk monomer density of $n_b\sigma^3$=0.1. (a) 10-mers. (b) 20-mers. In this case, predictions by the locally incompressible fluid approach (LIF), are also included. (c) 30-mers.

IV. DENSITY FUNCTIONAL THEORY RESULTS

A. Repulsive surfaces

We start by evaluating the GFD, TPTD1, and TPT1 approaches by comparing predictions with simulation data of interactions between repulsive surfaces. Such comparisons are given in Fig. 10. We see that the GFD and TPTD1 predictions are superior, although the TPT1 also performs reasonably satisfactorily. Between the two former versions, the GFD is slightly more accurate in the presence of 10-mers and 20-mers, while it underestimates the barrier more than the TPTD1 does, when the degree of polymerization is 30. The TPTD1 calculations display a somewhat too long-ranged depletion attraction, but the discrepancy is small. The accu-

racy of all approaches seems to deteriorate somewhat with chain length, although we should remember that the same statement presumably is true for the simulation data. We also noticed in Fig. 4 that the free-energy curves are much more sensitive to small deviations from the exact results than the corresponding osmotic pressure data are.

Finally, we have included predictions by the LIF functional in Fig. 10(b). As mentioned earlier, these predictions are primarily included to give an indication of differences between a locally incompressible (lattice) and globally incompressible (continuum) polymer solution model. The two approaches display the same qualitative features of the surface interaction ("depletion stabilisation") and even a reasonable quantitative agreement. In graph (c), we also display the interactions on a larger scale, on which the barriers are undetectable.

One might, at this stage, be inclined to believe that our simplistic choice of weight function for the coarse-grained density is a primary source of error in the density functional theory (DFT) calculations. However, at these low monomer densities, very similar results will be obtained irrespective of the choice of weight functions. A specific illustration will be provided in the next subsection.

B. Attractive surfaces

Density functional predictions of interaction free energies between adsorbing surfaces appear to be considerably more difficult than when these are nonadsorbing. Comparisons with simulation results are given in Fig. 11. Here, predictions by all our investigated versions of DFT are evaluated, including the GFD using the coarse-graining weight function suggested by Tarazona and Evans [36]. There are several things to be noted.

(i) The Chiew, Song, and TPT1 predictions essentially coincide. The agreement between them is in fact quite remarkable. Common to all of these is the neglect of specific end monomer excluded volume effects; i.e., they belong to our first category of functionals, with a structure given by Eq. (33).

(ii) The GFD and TPTD1 completely outperform their competitors. They still underestimate the free energy barrier by a factor of 1.2–1.8, but for the other versions this factor is in the range of 4–6. We saw earlier that there are some size dependence effects in the simulations, which may generate an overestimation of the barrier, but only slightly so.

(iii) The TPTD1 provides the best predictions of barrier heights, but also produces a somewhat too long-ranged repulsive tail.

(iv) The DFT calculations are rather insensitive to the choice of smoothing density weight functions. This is presumably because the average monomer density is relatively low.

(v) The LIF functional ("lattice approach") predicts a rather different behavior. Strictly speaking, it does predict a barrier, but it is hardly even noticeable on this scale and occurs at much too large separations. Given that we have highlighted these differences observed between continuum and lattice approaches, we did not include the LIF predictions in graph (b).

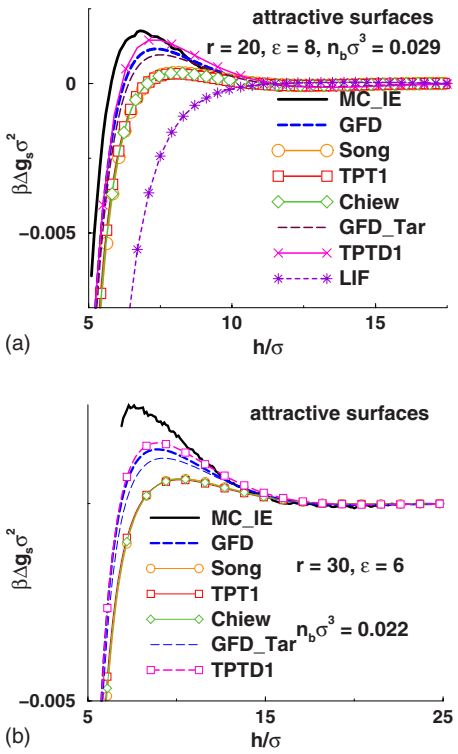

FIG. 11. (Color online) Comparisons between simulation results and density functional predictions of forces between attractive surfaces in the presence of semiflexible hard-sphere polymers. (a) 20-mers, $\epsilon=8$, $n_b\sigma^3=0.029$. (b) 30-mers, $\epsilon=6$, $n_b\sigma^3=0.022$.

Then, why do the GFD and TPTD1 perform so much better than the other investigated versions? It turns out that they do so because they take into account the extra volume that the end monomers exclude to the surrounding; i.e., they belong to our second category of functionals, Eq. (39). This is highlighted in Fig. 12, where GFD and TPTD1 predictions are compared with those obtained when the separate treatment of end monomers is excluded—i.e., the GFD-AME and TPTD1-AME versions. The end effect is quite clear and is particularly strong for TPTD1. There is a close agreement between the GFD-AME and TPT1 data, while the GFD predicts a substantially stronger barrier. The results in graph (b) are especially remarkable, since we find that the end effect is significant, even when each chain contains hundreds of monomers. We also note that while the TPTD1, as expected, predicts the highest free-energy barrier in the presence of 30-mers, the value of this quantity is essentially identical between GFD and TPTD1 when the chains are longer ($r=200$). The TPTD1 does, however, still predict a more long-ranged repulsive tail. Our simulation results on shorter chains imply that the GFD predictions are more accurate in this regime. Taking the extra volume excluded by end monomers into account will, at strongly adsorbing surfaces, tend to push these monomers farther away from the surfaces than in corresponding models where this extra excluded volume is disregarded (not shown). This will in turn lead to a stronger excluded volume repulsion at the midplane between the surfaces, thus generating a more repulsive barrier.

The Song, Chiew, and TPT1 equations of states could, in a rather trivial manner, be used to formulate functionals of

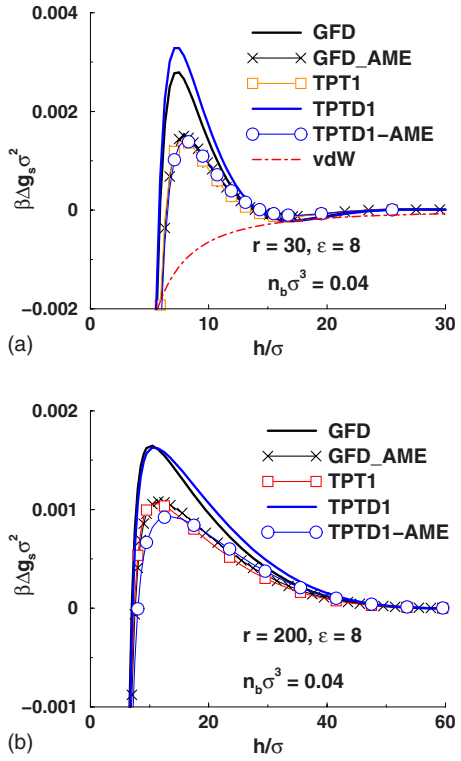

FIG. 12. (Color online) Comparing DFT approaches employing Eqs. (33) and Eq. (39) for the excess part of the free-energy functional. The former does not discriminate between monomers, whereas the second takes into account that end monomers exclude more volume than the others. TPT1, GFD-AME, and TPTD1-AME belong to the first category, while TPTD1 and GFD belong to the second. The surfaces are attractive, the stiffness parameter is $\epsilon=8$, and the bulk monomer density is $n_b\sigma^3=0.04$. (a) 30-mers. (b) 200-mers.

the form given by Eq. (39). This is easily achieved by separately extracting the respective predictions of the excess free energy per monomer for a dimer fluid. However, given their formal structure, using the monomer fluid as a reference, such a procedure is rather artificial. Still, our results suggest that it might lead to improved functionals.

We end with two figures summarizing our major findings regarding the influence of monomer concentration and intrinsic chain stiffness, on the interaction between adsorbing surfaces. The DFT qualitatively reproduces the response observed in simulations. It has also the advantage of computational speed and an exact knowledge of the bulk monomer density. This allows us to present a clearer and more condensed picture of the observed effects.

In Fig. 13, we have maintained the intrinsic chain stiffness, while we change the bulk monomer concentration. We see how the barrier at low concentrations, due to overlap between tails of adsorbed chains, initially increases with density. Finally, the interaction becomes attractive as a consequence of surface saturation and the concurrent depletion of nonadsorbed chains.

Another option is to maintain a constant bulk monomer concentration and monitor how the surface interactions respond to changes of chain rigidity. This is illustrated in Fig.

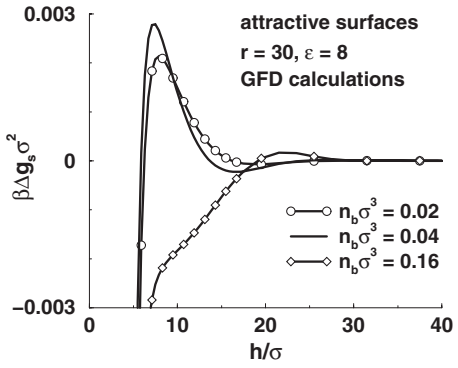

FIG. 13. A summary of the qualitative response of the interaction between adsorbing surfaces to changes of the bulk monomer concentration. The solution contains semiflexible 30-mers, with $\epsilon=8$.

14. An additional advantage with the DFT approach is that it is easy, and computationally cheap, to include the solvent explicitly. In Fig. 14(b), we provide corresponding surface interactions in the presence of a hard-sphere solvent, where the solvent particles have the same diameter as the monomers. We assume that the surfaces have no solvent affinity; i.e., the solvent particles only sense the repulsive part of the surface potential. It is gratifying to find that the qualitative behavior we find in our implicit solvent model is preserved

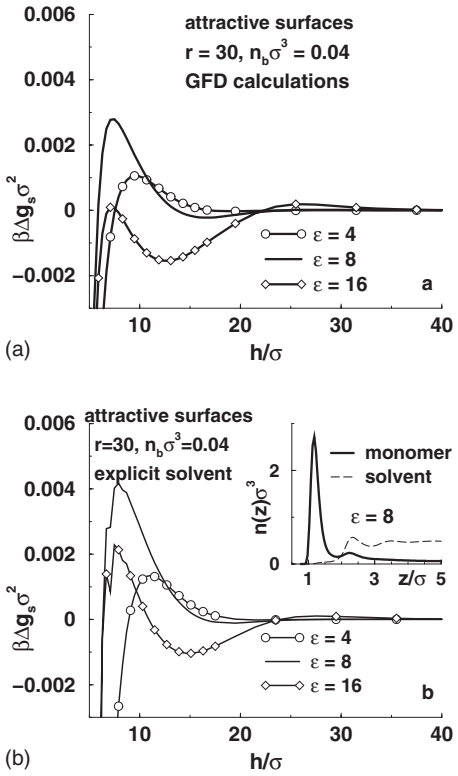

FIG. 14. A summary of the response of the interaction between adsorbing surfaces to changes of the intrinsic chain stiffness using explicit and implicit solvent models. The solution contains semiflexible 30-mers, with $n_b\sigma^3$. (a) Implicit solvent. (b) Explicit solvent.

when the solvent is treated explicitly, at least if it enters in the described manner. Quantitatively, we do observe a significantly stronger free-energy barrier with the explicit solvent model.

V. CONCLUSIONS

We have successfully simulated interactions between surfaces, either adsorbing or nonadsorbing, immersed in polymer solutions containing semiflexible hard-sphere chains. A McMillan-Mayer approach was adopted; i.e., the solvent was not included explicitly. Both the grand canonical ensemble and the isotension ensemble, coupled with perturbation techniques, have been utilized and compared. We found the grand canonical ensemble to be preferable when the surface are nonadsorbing. In the case of strongly adsorbing surfaces and stiff polymers, however, that approach fails almost completely. In those cases, and if high precision and accuracy is desired, the isotension ensemble method is the only viable option. The GCE approach is probably acceptable, if one settles with the overall appearance of the surface force curve, including the strong attraction at short range (cf. Fig. 8), and refrains from attempting to quantify free-energy barriers.

Switching focus to the investigated surface interactions, we have found a strong influence from the intrinsic rigidity of the dissolved polymers. Increasing the intramolecular chain stiffness from fully flexible to moderately stiff chains leads to an increased free energy barrier. This qualitative response is found for attractive as well as repulsive surfaces. Interactions between strongly adsorbing surfaces were more closely investigated. Here, we found that a further increased stiffness, to very rigid chains, leads to a diminished free-energy barrier and even a long-ranged attraction. This is due to the surfaces being saturated by a strong adsorption of rigid chains. The attraction at long range is thus caused by the depletion of nonadsorbed chains.

Finally, we made rather extensive comparisons with various versions of Woodward's polymer density functional theory. These versions differ by the approximate way in which excluded volume interactions are taken into account. In our case, the excess free energy per monomer is (with one exception) derived by integration of a polymer fluid equation of state. Two such equations of state uses a dimer fluid as "reference," which in a natural way leads to a separate description of the (larger) volume excluded by the end monomers in a chain. By comparing surface force predictions with corresponding simulation data, we established that these equations of state, the GFD and TPTD1, are superior to the others, at least for the model systems investigated. We also found that a separate treatment of the end monomer excluded volume has substantial effects on the predicted surface forces, even when each dissolved polymer contains hundreds of monomers. Other equations of state that use a monomer reference fluid could in principle also be described by functionals treating the end monomers specifically. However, this approach is in those cases somewhat artificial. At any rate, the performances of the GFD and TPTD1 functionals are comparable, with an almost quantitative accuracy when the surfaces are non-adsorbing. The accuracy is poorer for strongly adsorbing surfaces, but is still reasonable. Simulated responses of the surface interactions to changes of the various investigated system parameters are qualitatively reproduced by virtually all the density functional versions we have studied. A possible exception is the density functional analog of the Sheutjens-Fleer theory, adopting a locally incompressible polymer solution model. In this case, the barriers are predicted to be considerably weaker and located at much larger separations.

[1] M. Ruths, H. Yoshizawa, L. J. Fetters, and J. N. Israelachvili, Macromolecules **29**, 7193 (1996).
[2] T. Kuhl, Y. Guo, J. L. Alderfer, A. D. Berman, D. Leckband, J. N. Israelachvili, and S. Wen Hui, Langmuir **12**, 3003 (1996).
[3] T. Kuhl, A. D. Berman, S. Wen Hui, and J. N. Israelachvili, Macromolecules **31**, 8250 (1998).
[4] T. Kuhl, A. D. Berman, S. Wen Hui, and J. N. Israelachvili, Macromolecules **31**, 8258 (1998).
[5] H.-W. Hu and S. Granick, Macromolecules **23**, 613 (1990).
[6] M. Seitz, C. K. Park, J. Y. Wong, and J. N. Israelachvili, Langmuir **17**, 4616 (2001).
[7] G. Sun, M. Kappl, and H.-J. Butt, Colloids Surf., A **250**, 203 (2004).
[8] M. Müller and W. Paul, J. Chem. Phys. **100**, 719 (1994).
[9] S. K. Kumar, I. Szleifer, and A. Z. Panagiotopoulos, Phys. Rev. Lett. **66**, 2935 (1991).
[10] K. K. Mon and B. Griffiths, Phys. Rev. A **31**, 956 (1985).
[11] M. N. Rosenbluth and A. W. Rosenbluth, J. Chem. Phys. **23**, 356 (1955).
[12] J. Harris and S. Rice, J. Chem. Phys. **88**, 1298 (1988).
[13] J. I. Siepmann and D. Frenkel, Mol. Phys. **75**, 59 (1992).
[14] D. Frenkel, G. C. A. M. Mooij, and B. Smit, J. Phys.: Condens. Matter **3**, 3053 (1992).
[15] D. Frenkel and B. Smit, *Understanding Molecular Simulations* (Academic Press, San Diego, 1996).
[16] J. J. de Pablo, M. Laso, and U. W. Suter, J. Chem. Phys. **96**, 2395 (1992).
[17] J. J. de Pablo, M. Laso, and U. W. Suter, J. Chem. Phys. **96**, 6157 (1992).
[18] M. Parinello and A. Rahman, Phys. Rev. Lett. **45**, 1196 (1980).
[19] B. Svensson and C. E. Woodward, J. Chem. Phys. **100**, 4575 (1994).
[20] B. Svensson and C. E. Woodward, Mol. Phys. **87**, 1363 (1996).
[21] J. Forsman and C. E. Woodward, Mol. Phys. **90**, 637 (1997).
[22] C. H. Bennett, J. Comput. Phys. **22**, 245 (1976).
[23] A. Czezowski and C. E. Woodward, Comput. Phys. Commun. **142**, 117 (2001).
[24] A. Broukhno, T. Åkesson, B. Jönsson, and P. Vorontsov-Velyaminov, J. Chem. Phys. **113**, 1 (2000).
[25] B. Jönsson, A. Broukhno, J. Forsman, and T. Åkesson, Lang-

muir **19**, 9914 (2003).
[26] J. Forsman, A. Broukhno, B. Jönsson, and T. Åkesson, J. Chem. Phys. **120**, 413 (2004).
[27] C. E. Woodward, J. Chem. Phys. **94**, 3183 (1991).
[28] R. Y. Rubinstein, *Simulation and Monte Carlo Methods* (Wiley, New York, 1981).
[29] G. Deitrick, L. Scriven, and H. Davis, J. Chem. Phys. **90**, 2370 (1989).
[30] J. Forsman and C. E. Woodward, Mol. Simul. **19**, 85 (1997).
[31] M. K. Fenwick and F. A. Escobedo, J. Chem. Phys. **120**, 3066 (2004).
[32] T. L. Hill, *An Introduction to Statistical Thermodynamics* (Dover, New York, 1986).
[33] C. E. Woodward and A. Yethiraj, J. Chem. Phys. **100**, 3181 (1994).
[34] J. Forsman and C. E. Woodward, J. Chem. Phys. **119**, 1889 (2003).
[35] S. Nordholm, M. Johnson, and B. C. Freasier, Aust. J. Chem. **33**, 2139 (1980).
[36] P. Tarazona and R. Evans, Mol. Phys. **52**, 847 (1984).
[37] Y. C. Chiew, Mol. Phys. **70**, 129 (1990).
[38] Y. Song, S. M. Lambert, and J. M. Prausnitz, Macromolecules **27**, 441 (1994).
[39] T. Boublik, J. Chem. Phys. **53**, 471 (1970).
[40] G. A. Mansoori, N. F. Carnahan, K. E. Starling, and T. W. Leland, J. Chem. Phys. **54**, 1523 (1971).
[41] J. K. Percus and G. J. Yevick, Phys. Rev. **110**, 1 (1958).
[42] M. S. Wertheim, J. Chem. Phys. **87**, 7323 (1987).
[43] D. Cao and J. Wu, J. Chem. Phys. **121**, 4210 (2004).
[44] K. G. Honnell and C. K. Hall, J. Chem. Phys. **95**, 4481 (1991).
[45] R. Dickman and C. K. Hall, J. Chem. Phys. **85**, 4108 (1986).
[46] J. M. Wichert, H. S. Gulati, and C. K. Hall, J. Chem. Phys. **105**, 7669 (1996).
[47] J. Chang and S. I. Sandler, Chem. Eng. Sci. **49**, 2777 (1994).
[48] J. M. H. M. Scheutjens and G. J. Fleer, Macromolecules **18**, 1882 (1985).
[49] J. Forsman, C. E. Woodward, and B. C. Freasier, J. Chem. Phys. **118**, 7672 (2003).
[50] M. Müller, J. Chem. Phys. **116**, 9930 (2002).
[51] J. Forsman and C. E. Woodward, Macromolecules **39**, 1261 (2006).
[52] J. Forsman and C. E. Woodward, Macromolecules **39**, 1269 (2006).